Modeling generalized parton distributions to describe deeply virtual Compton scattering data

A. Freund
Institut für Theoretische Physik, Universität Regensburg, D-93040 Regensburg, Germany

M. McDermott
Division of Theoretical Physics, Department of Mathematical Sciences, University of Liverpool, Liverpool, L69 3BX, United Kingdom

M. Strikman
The Pennsylvania State University, Department of Physics, University Park, Pennsylvania 16802
(Received 25 September 2002; published 10 February 2003)

We present a new model for generalized parton distributions (GPDs), based on the aligned jet model, which successfully describes the deeply virtual Compton scattering (DVCS) data from H1, ZEUS, HERMES and CLAS. We also present an easily implementable and flexible algorithm for their construction. This new model is necessary since the most widely used models for GPDs, which are based on factorized double distributions, cannot, in their current form, describe the DVCS data when employed in a full QCD analysis. We demonstrate explicitly the reason for the shortcoming in the data description. We also highlight several nonperturbative input parameters which could be used to tune the GPDs, and the t dependence, to the DVCS data using a fitting procedure.

DOI: 10.1103/PhysRevD.67.036001 PACS number(s): 11.10.Hi, 11.30.Ly, 12.38.Bx

I. INTRODUCTION

Generalized parton distributions (GPDs) have been studied extensively in recent years [1–12]. This interest was spurred by the realization that these distributions are not only the basic, nonperturbative ingredients in hard, exclusive processes such as deeply virtual Compton scattering (DVCS), or exclusive vector meson production, but that they are generalizations of the well known parton distribution functions (PDFs) from inclusive reactions. GPDs incorporate both a partonic and a distributional amplitude behavior and hence contain more information about the hadronic degrees of freedom than PDFs. In fact, GPDs are true two-parton correlation functions, allowing access to the highly non-trivial parton correlations inside hadrons [13].

GPDs can be broadly characterized by the following features.

They depend on two momentum fraction variables, a partonic variable defined with respect to either the incoming or the average of the incoming and outgoing proton momentum and the *skewedness* (which is the difference between the momentum fractions of two adjacent partons in the parton ladder).

For fixed skewedness, they are continuous functions of the dependent variable and span two distinct regions, the Dokshitzer-Gribov-Lipatov-Altarelli-Parisi (DGLAP) region and the Efremov-Radyushkin-Brodsky-Lepage (ERBL) region, in which their evolution in scale obeys generalized versions of the DGLAP and ERBL evolution equations, respectively, and in which their behavior is qualitatively different.

They are even functions of the skewedness variable and the singlet, non-singlet and gluon distributions are either symmetric or anti-symmetric about the center point of the ERBL region (the symmetry obeyed depends on the precise definitions used).

The Lorentz structure of their definitions implies a polynomiality condition [2,3,11,14]: their $(N-1)$th moments are polynomials in the square of the skewedness of degree no greater than $N/2$.

They reduce to the ordinary PDFs in the limit of zero skewedness (the ''forward limit'').

All of the above features have to be preserved under evolution in scale.

Any suggested model of GPDs should adhere to these mathematical features. In [16] such a model, based on double distributions (DDs), was suggested for the GPD input distributions (see also [17]). In [14] it was realized that an additional term, the so-called D term, was required in the ERBL region for the unpolarized quark singlet and gluon distributions in order to satisfy polynomiality for even N. The use of factorized [15] DDs augmented with a D term has become a popular phenomenological model. Unfortunately, when this type of model for input GPDs was used in its current form to calculate deeply virtual Compton scattering at both leading (LO) and next-to-leading order (NLO), the results were not in agreement with the H1 data [18] on the DVCS photon level cross section, $\sigma(\gamma^* p \to \gamma p)$, and the HERMES and CLAS data [19] on the DVCS single spin asymmetry or charge asymmetry [20–22].

Another popular model for input GPDs, inspired by the aligned jet model (AJM) [23] and its QCD extension [24], is based on the observation that at a scale $Q^2 \sim 1$–2 GeV^2 and a wide range of x_{bj}, soft physics gives the dominant contribution to the parton densities. As a result the effect of skewedness at small x_{bj} should be rather small and hence at the input scale it is a good approximation to set the GPDs equal to the forward PDFs at the same parton fraction, X, defined with respect to the *incoming* proton [8] (for any skewedness). This has the advantage that it automatically satisfies the requirements of polynomiality for the first two moments; however one encounters infinities in the quark singlet GPD in the middle of the ERBL region.

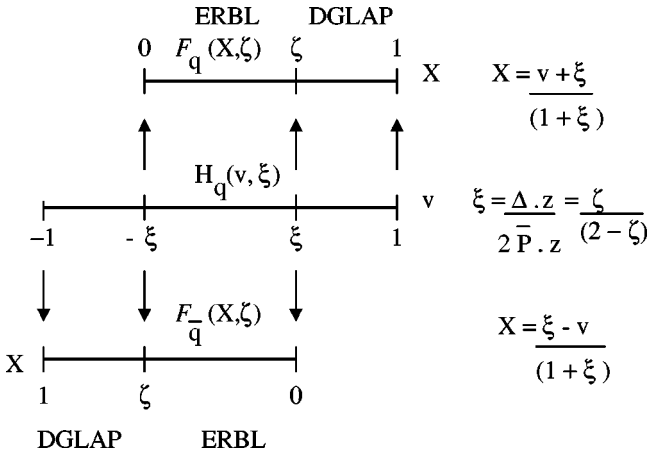

FIG. 1. The relationship between $\mathcal{F}^q(X,\zeta)$, $\mathcal{F}^{\bar{q}}(X,\zeta)$ and Ji's function $H^q(v,\xi)$ with $v\in[-1,1]$ and $X\in[0,1]$.

Another ''forward model,'' which may be considered to be an extreme case of a DD model, was adopted in [11] where one assumes that the GPD is equal to the forward PDF at the same parton momentum fraction, v, with respect to the average of the *incoming and outgoing* proton momentum $\bar{P}=(p+p')/2$ which implicitly contains the skewedness. This translates to an X which is shifted to lower values by an amount controlled by the skewedness. This ansatz works fine for the DGLAP region. Unfortunately in the ERBL region it also involves sampling the forward PDFs right the way down to zero in momentum fraction where they have not yet been measured (this is especially problematic for singular quark distributions). In this paper we construct an alternative, finite ''forward model'' for the input GPDs, using the forward input PDFs in the DGLAP region and imposing a simple form in the ERBL region that has the correct symmetries and ensures that polynomiality is respected in the first two moments (see [11] for alternative ways of dealing with this problem). As we will demonstrate this forward model reproduces the available data on DVCS reasonably well.

Throughout this paper we will use the off-diagonal representation of GPDs, $\mathcal{F}^i(X,\zeta)$, defined by Golec-Biernat and Martin [10] and used, for example, in the numerical solution of the GPD evolution equations in [25] (see [10,26,27] for other approaches to numerical evolution). They depend on the momentum fraction $X\in[0,1]$ of the incoming proton's momentum, p, and the skewedness variable $\zeta=\Delta^+/p^+$ (so that $\zeta=x_{bj}$ for DVCS). For the quark case, the relationship of the quark and anti-quark distributions, $\mathcal{F}^q(X,\zeta)$,$\mathcal{F}^{\bar{q}}(X,\zeta)$, to Ji's GPD $H^q(v,\xi)$ is shown in Fig. 1 with $\xi=\Delta^+/2\bar{P}^+$. More explicitly, for $v\in[-\xi,1]$,

$$\mathcal{F}^{q,a}\left(X=\frac{v+\xi}{1+\xi},\zeta\right)=\frac{H^{q,a}(v,\xi)}{1-\zeta/2}, \tag{1}$$

and for $v\in[-1,\xi]$

$$\mathcal{F}^{\bar{q},a}\left(X=\frac{\xi-v}{1+\xi},\zeta\right)=-\frac{H^{q,a}(v,\xi)}{1-\zeta/2}. \tag{2}$$

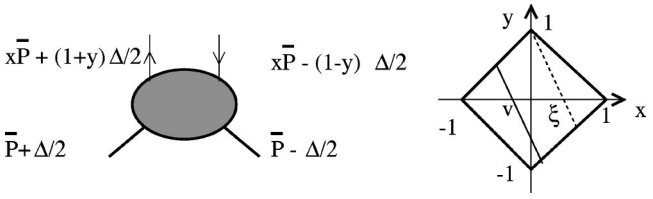

FIG. 2. Symmetric double distributions (left), indicating momentum fractions of the outgoing and returning partons, and (right) their physical domain.

The two distinct transformations between v and X for the quark and anti-quark cases are shown explicitly on the left hand side of Eqs. (1),(2) . There are two distinct regions: the DGLAP region, $X>\zeta$ ($|v|>\xi$), and the ERBL region, $X<\zeta$ ($|v|<\xi$). In the ERBL region, due to the fermion symmetry, $\mathcal{F}^q$ and $\mathcal{F}^{\bar{q}}$ are not independent. In fact $\mathcal{F}^q(X,\zeta)=-\mathcal{F}^q(\zeta-X,\zeta)$, which leads to an anti-symmetry of the unpolarized quark singlet distributions (summed over flavor a), $\mathcal{F}^S=\Sigma_a\mathcal{F}^{q,a}+\mathcal{F}^{\bar{q},a}$, about the point $\zeta/2$ (the non-singlet and the gluon, $\mathcal{F}^g$, which is built from $vH^g_{ji}(v,\xi)$, are symmetric about this point). $\mathcal{F}^{NS,g}$ are constructed analogously to $\mathcal{F}^S$ from $H^{NS,g}$.

The rest of the paper is organized as follows. Section II contains a detailed explanation of why DD-based models in their current form cannot describe the data. In Sec. III we construct our alternative forward model for input GPDs, which is motivated by the AJM [23,24] and describes the data well. In Sec. IV we propose a phenomenological model for the slope of the t dependence in which the slope parameter is allowed to change with photon virtuality, $q^2=-Q^2$. The model improves the theoretical description of the Q^2 dependence of the HERA data, relative to using a constant slope. Finally we summarize our findings in Sec. V.

II. THE PROBLEM WITH DOUBLE DISTRIBUTION MODELS

In this section we discuss factorized double distribution based models for GPDs and explain in detail why the sampling of the forward PDF at extremely small x in constructing the GPD leads to a problem in the quark singlet GPD.

Symmetric DDs, $F_{DD}(x,y,t,Q^2)$, were introduced in [3] with plus momentum fractions, x,y, of the outgoing and returning partons defined as shown in the left hand plot of Fig. 2. They exist on the diamond-shaped domain shown to the right of Fig. 2. The outgoing parton lines of course only have a single plus momentum relative to any particular external momenta, so the GPDs are related to these DDs via a reduction integral, involving $\delta(v-x-\xi y)$, along the off-vertical lines in the diamond (the dotted line corresponds to $v=\xi$):

$$H(v,\xi)=\int_{-1}^{1}dx'\int_{-1+|x'|}^{1-|x'|}dy'\,\delta(x'+\xi y'-v)F_{DD}(x',y'). \tag{3}$$

In [16,17] a model for $F_{DD}(x,y,t,\mu^2)$, at the input scale $\mu^2=Q_0^2$, was introduced in which the functional form is fac-

torized in x and y and in the t dependence, an assumption born out of convenience rather than physical necessity:

$$F^i_{DD}(x,y,\mu^2,t)=\pi^i(x,y)f^i(x,\mu^2)r^i(t). \tag{4}$$

Here f^i and r^i are the standard PDF and form factor for the parton distribution of general type i. Since the t dependence is assumed to factorize and thus of no importance to the following, we will suppress it from now on. The profile functions, $\pi^i(x,y)$, are asymptotic shape functions [3] for quarks and gluons of the general form

$$\pi(x,y)=\frac{\Gamma(2b+2)}{2^{2b+1}\Gamma^2(b+1)}\frac{[(1-|x|)^2-y^2]^b}{(1-|x|)^{2b+1}}, \tag{5}$$

and normalized such that

$$\int_{-1+|x|}^{1-|x|}dy\ \pi(x,y)=1. \tag{6}$$

Note that π is an even function of both its arguments [28]. The power b controls the size of the skewing effects in the input GPD. Usually $b=1$ is chosen for the quarks, corresponding to maximum skewedness, whereas $b=2$ is chosen for the gluons. In the limit $b\to\infty$ there is no external skewedness effect; however, since in this limit, $H(v,\xi)=q(v)$, this translates into internal dependence on the skewedness $\mathcal{F}(X,\zeta)=q[(X-\zeta/2)/(1-\zeta/2)]/(1-\zeta/2)$. Note that a consequence of the above model is a ratio of GPD to PDF for the quark singlet in the DGLAP region at $X=\zeta=x_{bj}$ which is substantially larger than 1 [25,27] for all experimentally relevant values of x_{bj}.

Concerning the description of the data using the above model, it was shown in [21] that maximal skewing ($b=1$) at ''conventional'' input scales ($Q_0=1,2$ GeV) overshoots the H1 data by a factor of 6–10. It was also demonstrated that one can describe, in LO only, the H1 data without including skewedness effects at the input scale, $Q_0=2$ GeV, if one neglects evolution [22]. This simplification, however, is not warranted since we know that the effects of skewed evolution are much stronger in the region of $X\sim\zeta$ compared to forward evolution [8,25]. Note that this region strongly influences the cross section at small x_{bj} and some asymmetries at both small and large x_{bj} [29], if they are dominated by the imaginary part of the amplitude which is proportional to $\mathcal{F}^S(\zeta,\zeta)$ at LO (see for example [21] as well as [30–32]).

One may wonder whether one can come closer to the data by choosing a very low input scale and valencelike partons as in the Glück-Reya-Vogt (GRV) scenario [33], generating the rise of the parton distributions entirely through evolution. It turns out that choosing the canonical value of $b_q=1$ and GRV98 input distributions ($Q_0=0.51,0.63$ GeV in LO and NLO, respectively) the curves still overshoot the data considerably. Indeed, even if one tries to minimize the effect of the enhancement due to skewedness at the input scale, by choosing a large value of $b_q=100$, evolution still drives the prediction above the data by at least a factor of ~ 4. Since, for example, $d\sigma_{DVCS}\simeq|\mathcal{F}^S(\zeta,\zeta)|^2$, the large enhancement of the quark singlet GPD at $X=\zeta$ is the root of the problem in this model. As we will explain below the origin of the enhancement stems from sampling singular forward sea distributions at extremely small x in the DD-based model. To understand the last statement, one has to first establish the regions in x in which the PDFs are sampled in the double distribution model, particularly at small x.

First, having defined the model for the factorized double distribution in Eq. (4) one may then perform the y' integration in Eq. (3) using the delta function. This then modifies the limits on the x' integration according to the region concerned. For the DGLAP region $X>\zeta$ ($v>\xi$) one has for the quark GPD

$$\mathcal{F}^{q,a}(X,\zeta)=\frac{2}{\zeta}\int_{(X-\zeta)/(1-\zeta)}^{X}dx'\,\pi^q \times\left(x',\frac{2}{\zeta}(X-x')+x'-1\right)q^a(x'). \tag{7}$$

For the anti-quark GPD in the DGLAP region $X>\zeta$ ($v<-\xi$) one has

$$\bar{\mathcal{F}}^{q,a}(X,\zeta)=\frac{2}{\zeta}\int_{-X}^{(-X+\zeta)/(1-\zeta)}dx'\,\pi^q \times\left(x',-\frac{2}{\zeta}(X+x')+x'+1\right)\bar{q}^a(|x'|). \tag{8}$$

Changing variables from $x\to -x$ and exploiting the fact that the profile functions are even in both arguments one arrives at

$$\bar{\mathcal{F}}^{q,a}(X,\zeta)=\frac{2}{\zeta}\int_{(X-\zeta)/(1-\zeta)}^{X}dx'\,\pi^q \times\left(x',\frac{2}{\zeta}(X-x')+x'-1\right)\bar{q}^a(|x'|), \tag{9}$$

so that the singlet and non-singlet quark distributions are given by

$$\mathcal{F}^S(X,\zeta)=\sum_a\ \mathcal{F}^{q,a}+\bar{\mathcal{F}}^{q,a}=\sum_a\ \frac{2}{\zeta}\int_{(X-\zeta)/(1-\zeta)}^{X}dx'\,\pi^q \times(x',\tilde{y}(x'))[q^a(x')+\bar{q}^a(x')],$$

$$\mathcal{F}^{NS,a}(X,\zeta)=\mathcal{F}^{q,a}-\bar{\mathcal{F}}^{q,a}=\frac{2}{\zeta}\int_{(X-\zeta)/(1-\zeta)}^{X}dx'\,\pi^q(x',\tilde{y}(x')) \times[q^a(x')-\bar{q}^a(x')], \tag{10}$$

where $\tilde{y}(x')=2(X-x')/\zeta+x'-1$.

In the ERBL region, $X<\zeta$ ($|v|<\xi$) integration over y leads to

$$\mathcal{F}^{q,a}(X,\zeta)=\frac{2}{\zeta}\Bigg[\int_0^X dx'\,\pi^q\Big(x',\frac{2}{\zeta}(X-x')+x'-1\Big)q^a(x') - \int_{X-\zeta}^0 dx'\,\pi^q\Big(x',\frac{2}{\zeta}(X-x')+x'-1\Big) \times\overline{q}^a(|x'|)\Bigg],$$

$$\mathcal{F}^{\overline{q},a}(X,\zeta)=-\frac{2}{\zeta}\Bigg[\int_0^{\zeta-X} dx'\,\pi^q\Big(x',-\frac{2}{\zeta}(X+x')+x'+1\Big) \times q^a(x')-\int_{-X}^0 dx'\,\pi^q\Big(x',-\frac{2}{\zeta}(X+x') +x'+1\Big)\overline{q}^a(|x'|)\Bigg]. \tag{11}$$

Again, using $x\to -x$ and $\pi(|x'|,|y'|)$, one gets

$$\mathcal{F}^{q,a}(X,\zeta)=\frac{2}{\zeta}\Bigg[\int_0^X dx'\,\pi^q(x',\tilde{y}(x'))q^a(x') - \int_0^{\zeta-X} dx'\,\pi^q(x',\tilde{y}(-x'))\overline{q}^a(x')\Bigg],$$

$$\mathcal{F}^{\overline{q},a}(X,\zeta)=-\frac{2}{\zeta}\Bigg[\int_0^{\zeta-X} dx'\,\pi^q(x',\tilde{y}(-x'))q^a(x') - \int_0^X dx'\,\pi^q(x',\tilde{y}(x'))\overline{q}^a(x')\Bigg]. \tag{12}$$

Hence, for the singlet and non-singlet combinations one has

$$\mathcal{F}^S(X,\zeta)=\sum_a\ \mathcal{F}^{q,a}+\mathcal{F}^{\overline{q},a}=\sum_a\ \frac{2}{\zeta}\Bigg[\int_0^X dx'\,\pi^q(x',\tilde{y}(x')) \times[q^a(x')+\overline{q}^a(x')]-\int_0^{\zeta-X} dx'\,\pi^q(x',\tilde{y}(-x')) \times[q^a(x')+\overline{q}^a(x')]\Bigg],$$

$$\mathcal{F}^{NS,a}(X,\zeta)=\mathcal{F}^{q,a}-\mathcal{F}^{\overline{q},a}=\frac{2}{\zeta}\Bigg[\int_0^X dx'\,\pi^q(x',\tilde{y}(x')) \times[q^a(x')-\overline{q}^a(x')] + \int_0^{\zeta-X} dx'\,\pi^q(x',\tilde{y}(-x')) \times[q^a(x')-\overline{q}^a(x')]\Bigg]. \tag{13}$$

These expressions clearly satisfy the correct symmetry properties, i.e., $F^S(\zeta-X,\zeta)=-F^S(X,\zeta)$, $F^{NS,a}(\zeta-X,\zeta)=F^{NS,a}(X,\zeta)$ [note that $\tilde{y}(x')\to\tilde{y}(-x')$ when $X\to\zeta-X$]. Analogously for the gluon one obtains

$$\mathcal{F}^g(X,\zeta)=\frac{2}{\zeta}\int_{(X-\zeta)/(1-\zeta)}^X dx'\,\pi^g(x',\tilde{y}(x'))x'g(x') \tag{14}$$

for the DGLAP region, and

$$\mathcal{F}^g(X,\zeta)=\frac{2}{\zeta}\Bigg[\int_0^X dx'\,\pi^g(x',\tilde{y}(x'))x'g(x') + \int_0^{\zeta-X} dx'\,\pi^g(x',\tilde{y}(-x'))x'g(x')\Bigg] \tag{15}$$

for the ERBL region (which is symmetric under $X\to\zeta-X$).

Inspection of the integration limits in Eqs. (10),(13) highlights the main problem. In the limit $X\to\zeta$, as a result of the lower limits of the integrals the forward PDF is sampled closer and closer to $x'=0$, where it has not yet been measured. This will be irrelevant providing the integrand is sufficiently non-singular in x' in this region i.e. it can happen if the profile functions, π^i, provide a strong suppression of this region, or if the PDFs themselves are sufficiently non-singular. However, we know that phenomenological quark and sometimes even gluon input distributions are singular in the small x region. In the quark case this problem is made worse by the fact that we sample the number distribution $q(x')$ rather than the momentum distribution $x'q(x')$ (so that a non-singular momentum distribution $xq(x)\propto x^a$ for $a\in[0,1]$ will give a singular number distribution $q(x)\propto x^{a-1}$).

It turns out that for realistic quark distributions the region close is $x'=0$ is very significantly sampled for small $\zeta=x_{bj}$. This leads to two serious problems. First, the forward distributions are unknown here so one must extrapolate the ''known'' analytic forms downward in x'. Secondly, and much more importantly, it leads to a very significant enhancement of the quark singlet GPDs relative to the PDFs for $X\approx\zeta$, i.e., the region most relevant for DVCS. Though of paramount importance for DVCS, this region is but a small region of phase space where the current factorized DD models fail.

We illustrate this using a series of three figures relating to the formation of the quark singlet GPD in the DGLAP region close to $X=\zeta$. Figure 3 shows the integrand, $I(x')=\pi^u(x',\tilde{y})\,u^S(x')$, of Eq. (10) for the up quark singlet (multiplied by ζ) as a function of x'/ζ for two values of $\zeta=0.1,0.0001$ and two values of $X-\zeta=0.1,0.001$. Clearly as X approaches ζ the PDF is sampled at progressively smaller values of $x'\ll\zeta$, where for small ζ it is unknown. Figure 4 shows the average value of x' sampled in this integral (divided by ζ) as a function of ζ for several values of $X-\zeta$. For very small values of $X-\zeta$ the average value of x' settles down to about $\zeta/4$, for small ζ. Finally in Fig. 5 we show, for Martin-Roberts-Stirling-Thorne (MRST) input PDFs, the ratio of the quark singlet GPD to PDF at $\zeta=0.0001,0.1$, for the canonical value of the power, $b_q=1$, in Eq. (5). Note the large enhancement of the GPD at $X\approx\zeta$, particularly for small ζ in the upper plot. We emphasize that this enhance-

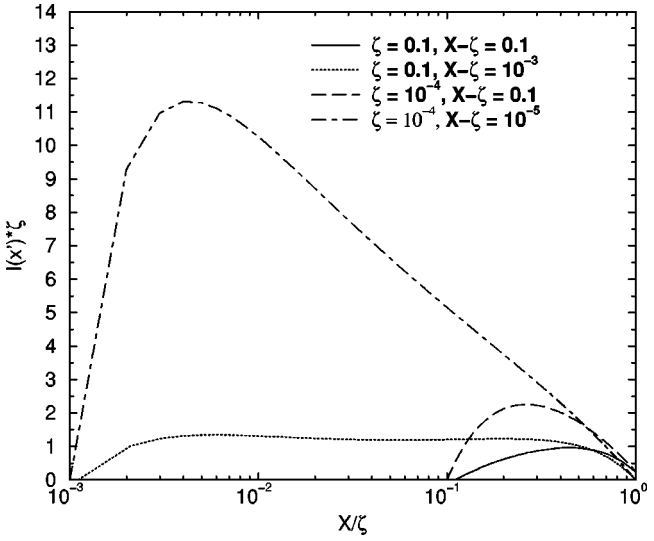

FIG. 3. The integrand of Eq. (10), illustrating how the up singlet PDF is sampled in the DGLAP region close to the boundary of the ERBL region, to produce the up singlet GPD.

ment, which leads to an overshoot of the DVCS data, is built in right at the start in the modeling of the quark singlet GPD at the input scale. One also sees that for the gluon, which uses $x'g(x')$, and $b_g=2$, the ratio remains close to unity.

The most important enhancement effect in the valence region, $\zeta \gtrsim 0.1$, originates from the relative shift of the parton momentum fraction X to smaller values close to $X=\zeta$ (although the enhancement from small $\langle x' \rangle$ is still significant). As we will show in the next section, the assumption that $H(v,\xi)=(1-\zeta/2)\mathcal{F}(X,\zeta)=q(v)$ with $v=(X-\zeta/2)(1-\zeta/2)$ gives a good description of the data at both small and large x_{bj}. As stated before, this corresponds to a factorized DD model with $b=\infty$, i.e., with no external skewedness. However, in terms of a comparison of GPD to forward PDF,

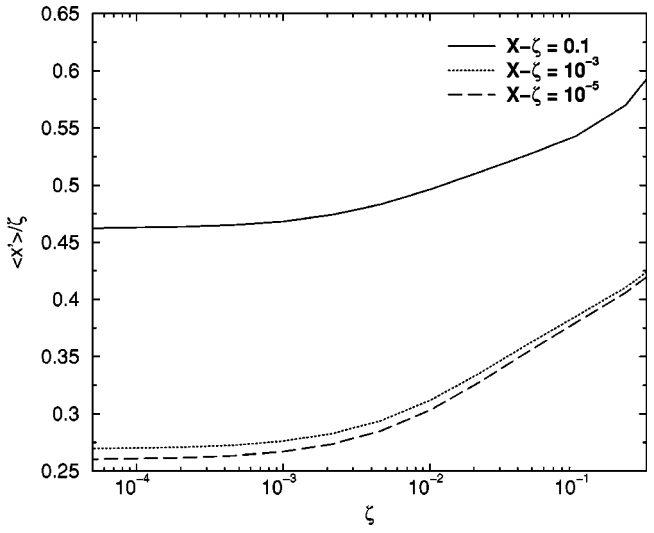

FIG. 4. The average value of x' sampled in the DGLAP region in the double distribution model, for the up singlet GPD, close to the boundary with the ERBL region as a function of the skewedness. Several values of $X-\zeta$ are shown.

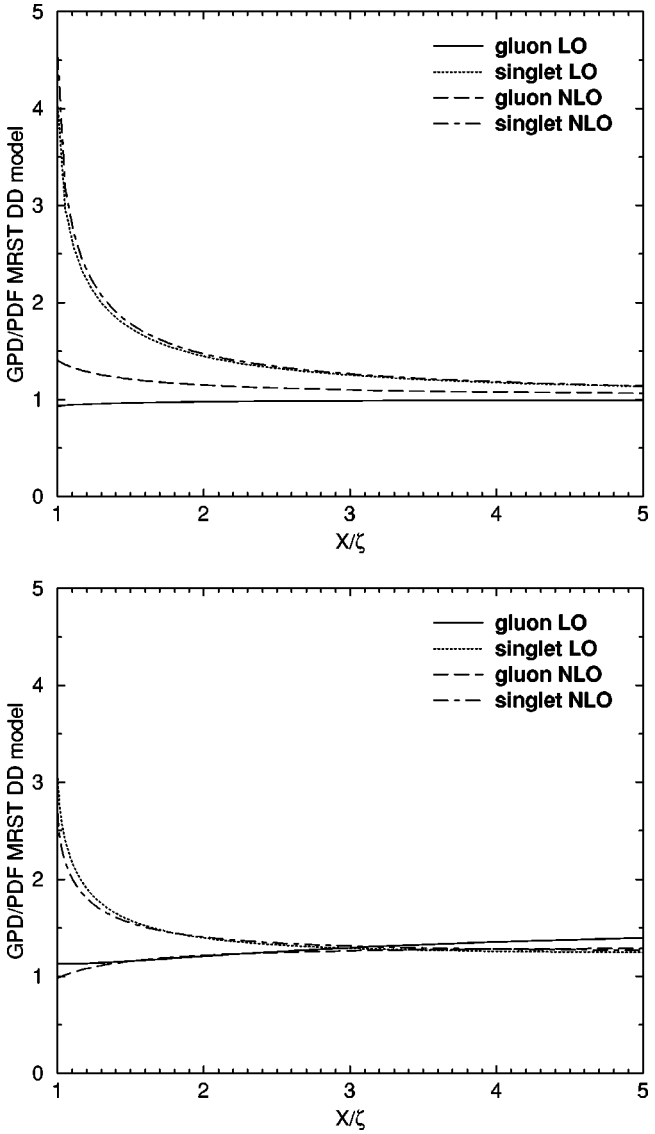

FIG. 5. The ratio GPD to PDF at $\zeta=0.0001$ (upper plot) and $\zeta=0.1$ (lower plot) for the quark singlet and gluon in the double distribution model, using MRST01 distributions in LO and NLO, at the input scale $Q_0=1$ GeV. Note the large enhancement of the quark singlet close to $X=\zeta$.

there is a residual effect of skewedness since one now has to compare $q(v)$ with $q(X)$. Since we are comparing number distributions which are more singular than momentum distributions, any shift in the momentum fraction to smaller values will lead to a quite a large enhancement of $q(v)$ relative to $q(X)$. For CTEQ6M, for example, the enhancement at $X=0.1$ and $\zeta=0.1$ is about 1.7 for the quark singlet, which increases further if more skewedness is added by decreasing b.

However, as we will demonstrate in Sec. III, the available data allow little room for further enhancement due to skewedness at the input scale since the LO result, at least, is already close to the upper bound of the experimental errors. Therefore, only the extremal "$b=\infty$" version of the current factorized DD model can be used to describe the data. An obvious solution to this is to modify the quark singlet profile

functions in Eq. (4) in such a way as to suppress the region of very small x'. However, one must find a new functional form which achieves this without spoiling the known mathematical features of GPDs discussed above. Alternatively, one abandons the attempt to model a DD using a factorized form $\pi(x,y)f(x)$, which though appealing due to its simplicity is possibly too simplistic in its form. This remains an open problem and has to be addressed by those who wish to use the double distribution framework, factorized or not, to model GPDs.

III. THE FORWARD INPUT MODEL AND THE ALIGNED JET MODEL

In this section we revisit the logic of setting the GPDs equal to the forward PDFs by proposing an alternative forward model to that suggested in [11], with suitably symmetrized input GPDs in the ERBL region constructed so as to satisfy the requirements of polynomiality for the first two moments.

In [9] DVCS was predicted to be measurable at the DESY-ep-collider-HERA and, allowing for the freedom associated with choosing the slope parameter, B, the predictions successfully describe both the H1 data [18] and the recent ZEUS result [34,35] on the photon-level DVCS cross section. This was achieved by modeling the imaginary part of the DVCS amplitude at the input scale using the aligned jet model [24]. This was then compared to the imaginary part of the deep inelastic scattering (DIS) amplitude, calculated within the same framework, which was found to be smaller by a factor of about two. The comparison enabled the normalization of the DVCS amplitude at the input scale to be set using F_2 structure function data. The DVCS amplitude was then evolved to higher scales using LO skewed evolution in perturbative QCD.

The basic relation between the DVCS and DIS amplitudes, using the AJM, is given by [9]

$$R=\frac{\mathrm{Im}\mathcal{T}_{\mathrm{DVCS}}}{\mathrm{Im}\mathcal{T}_{\mathrm{DIS}}}=\ln\left(1+\frac{Q^2}{M_0^2}\right)\left(1+\frac{M_0^2}{Q^2}\right)\simeq 1.5\text{–}2.5, \quad (16)$$

where Q^2 for the AJM is typically $1-3$ GeV^2 and M_0 is a hadronic scale which roughly corresponds to the lowest allowed, excited intermediate state in the s channel. Therefore, $M_0^2\sim 0.4\text{–}0.6$ GeV^2, or about m_ρ^2. The AJM neglects the contribution of quarks with large transverse momenta in the quark loop attached to the photons in the handbag diagram. Since the contribution of small transverse momenta is more symmetric than the one at large transverse momenta, the AJM may somewhat overestimate the effect of skewedness at the input scale. Equation (16) can be generalized to demonstrate how the forward limit $\mathrm{Im}\mathcal{T}_{\mathrm{DVCS}}=\mathrm{Im}\mathcal{T}_{\mathrm{DIS}}$ is achieved, i.e., how the skewedness effect is reduced by giving the outgoing photon a spacelike virtuality, $q'^2=-Q'^2$:

$$R=\frac{\mathrm{Im}\mathcal{T}_{\mathrm{DVCS}}}{\mathrm{Im}\mathcal{T}_{\mathrm{DIS}}}=\ln\left(\frac{1+Q^2/M_0^2}{1+Q'^2/M_0^2}\right)\frac{1+M_0^2/Q^2}{1-Q'^2/Q^2}. \quad (17)$$

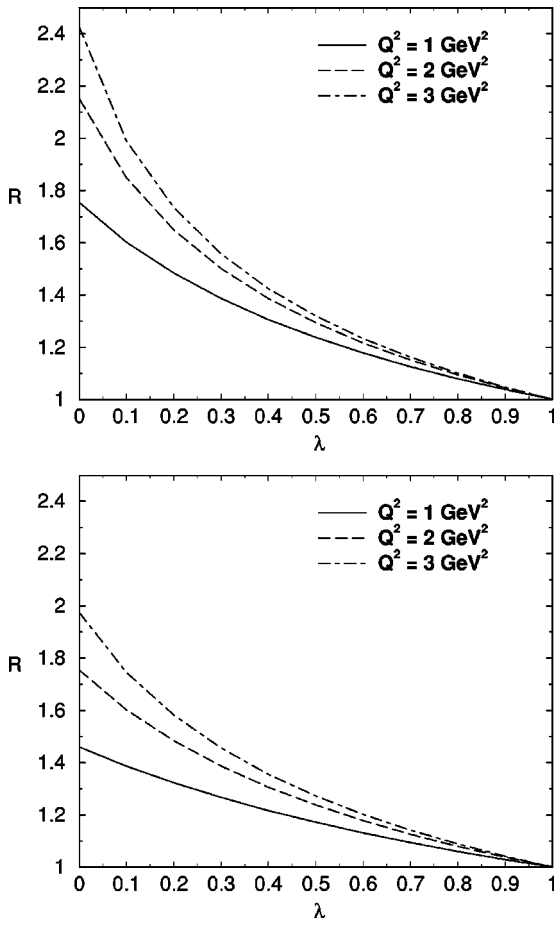

FIG. 6. The ratio R as a function of $\lambda=Q'^2/Q^2$ for several value of Q^2 and two values of $M_0^2=0.4$ GeV^2 (upper plot) and 0.8 GeV^2 (lower plot).

This procedure allows one to derive a very important relation between the relative momentum fractions of the outgoing and returning partons X and $-(X-\zeta)$ of the quark singlet GPD, and the virtualities of the incoming and outgoing photons

$$\lambda=\frac{X-\zeta}{X}=\frac{Q'^2}{Q^2}. \quad (18)$$

We illustrate this point in Fig. 6 by plotting R as a function of λ for several values of Q^2 and two values of M_0^2 to demonstrate the relative insensitivity of R (within 20–30 %) to M_0.

The plot shows that as X increases relative to ζ in the DGLAP region the ratio drops rapidly to its forward limit. For example, at $\lambda=1/2$, i.e., $X=2\zeta$, the curves are very flat and there is only a modest enhancement of 20–40 %. One also encounters this behavior in the DD model if one investigates the ratio of the GPD to the PDF in the DGLAP region (see for example [25,27]). It would therefore be advantageous to be able to directly relate R to a ratio of GPD to PDF. Trusting that perturbative QCD is applicable at the AJM input scale one can, in LO at least where the coefficient function is trivial, directly translate the ratio in amplitudes for a particular λ into a ratio of GPD to PDF:

$$R(\lambda)=\frac{\mathrm{Im}\mathcal{T}_{\mathrm{DVCS}}}{\mathrm{Im}\mathcal{T}_{\mathrm{DIS}}}=\frac{H^S(v=\xi(1+\lambda)/(1-\lambda),\xi)}{q^S(X)},$$

$$=\frac{\mathcal{F}^S(X=\zeta/(1-\lambda),\zeta)}{(1-\zeta/2)q^S(X)}, \tag{19}$$

i.e.,

$$\mathcal{F}^S(\zeta/(1-\lambda),\zeta)=(1-\zeta/2)R(\lambda)q^S(X). \tag{20}$$

There are several comments in order at this point: λ is now bounded from above through $\lambda\leqslant 1-\zeta$. This implies that the relationship between the ratios in Eq. (20) is only strictly true for $\lambda=0$ (i.e., for DVCS for which $Q'^2=0$). The case $\lambda\neq 0$ should be viewed as follows: for $Q^2\sim 2$ GeV^2, there is still the possibility of having more than one rung in the partonic ladder. Probing the uppermost rung with a virtuality Q^2 reveals the distribution in momentum fractions, in this case $X=\zeta$, i.e., $X-\zeta=0$ corresponding to $\lambda=0$. The next rung and its distribution in momentum fractions can be accessed by "emitting" a photon with spacelike virtuality (i.e., $Q'^2>0$). As Q'^2 increases and one goes further down the ladder to where $X\gg\zeta$, one approaches the forward limit. If one keeps the interpretation of the *s*-channel cut as being equal to the imaginary part of the "scattering" amplitude for $Q'^2\neq 0$, which, in LO, is directly proportional to GPD/PDF at $X\neq\zeta$ rather than at $X=\zeta$, then the ratio R is a direct measure of quark singlet GPD to the quark singlet PDF for $X\neq\zeta$. However, this logic is valid only at LO. At NLO, the situation radically changes since, first, the gluon directly enters into the amplitude, secondly, the convolution of the coefficient function with the GPD is no longer as trivial as in LO and thirdly, the value of α_s at low Q^2 is quite different in LO and NLO. Therefore such a simple relation as in Eq. (20) should and can no longer be valid. In order to keep the ansatz as simple as possible, we will only require that the model GPDs, at least in LO, produce a ratio, R, which is in broad agreement with the R values obtained in the AJM from Eq. (20).

If one chooses the forward model ansatz where the GPD equals the PDF at v in both LO and NLO, due to a lack of a better ansatz (see e.g. [11]),

$$H^S(v,\xi)=q^S(v)\equiv q^S\left(\frac{X-\zeta/2}{1-\zeta/2}\right), \tag{21}$$

which corresponds to the $b\to\infty$ limit of the DD model, one obtains a ratio of GPD to PDF at $X=\zeta$ of $\simeq 2.3$ for the quark singlet, in agreement with the AJM prediction although for slightly different values of Q_0^2 (directly compare the upper line in the upper plot of Fig. 6 with the quark singlet in Fig. 7 keeping in mind that $\lambda=0\Leftrightarrow X/\zeta=1$ and $\lambda=0.9\Leftrightarrow X/\zeta=10$). In consequence, our model ansatz corresponds to an AJM with maximal skewedness.

For our forward model in the DGLAP region we, therefore, choose for simplicity the ansatz of Eq. (21) for the quark singlet, the non-singlet (i.e., the valence) and the gluon. The ratios of GPD to PDF at the input scale for MRST01 quark singlet and gluon distributions [36] at LO and NLO at $Q_0=1$ GeV are shown in Fig. 7. For a function which falls as x decreases, such as the valence quark at small x or the MRST gluon at LO, this ansatz leads to a suppression of the point $X=\zeta$ relative to the forward case (see the solid line in Fig. 7). Note that in NLO the MRST gluon actually goes negative at small x, so a ratio of GPD to PDF >1 close to $X=\zeta$ in this case leads to a suppression of the DVCS cross section from the gluon contribution, relative to using PDFs. However, the DVCS cross section is rather insensitive to the behavior of this ratio close to $X=\zeta$ for the gluon, since it only enters in NLO, and is completely insensitive to it for the non-singlet quark case since this distribution only enters into the evolution.

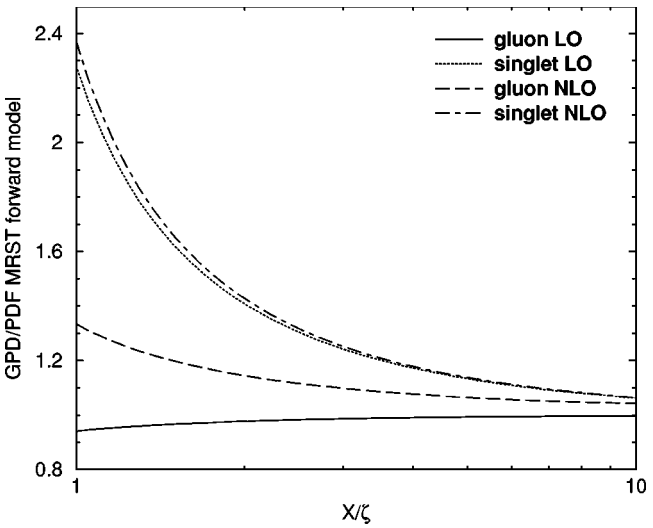

FIG. 7. The ratio GPD to PDF at $\zeta=0.0001$ for the quark singlet and gluon, using MRST01 distributions in LO and NLO, at the input scale $Q_0=1$ GeV. This ratio is weakly dependent on ζ, for small ζ.

The above reasoning indicates that the physics of the AJM model provides a guide for modeling input GPDs in the DGLAP region. If one compares the NLO imaginary part of the DVCS amplitude from the above model to the NLO imaginary part of the DIS amplitude as extracted from a recent H1 F_2 fit [42], we find for MRST2001 $R\simeq 3.8$ and for CTEQ6M, $R\simeq 2.7$ for $Q^2=3$ GeV^2 and $x=0.0005$. Because of the enhancement effect of evolution, the AJM result for R is basically reproduced for CTEQ6M but not for MRST2001 using Eq. (21). Given the widely different parametrizations at NLO, this seems acceptable to us, at present. As we will see below the enhancement effect generated through the shift is too strong for both LO and NLO at low values of Q^2 near the input scale.

The prescription in Eq. (21) does not dictate what to do in the ERBL region, which does not have a forward analogue. Naturally the GPDs should be continuous through the point $X=\zeta$ and should have the correct symmetries around the midpoint of the ERBL region. They are also required to satisfy the requirements of polynomiality:

$$M_N=\int_{-1}^{1}dv\,v^{N-1}[H^q(v,\xi)+H^g(v,\xi)]$$

$$= \sum_{k=0}^{N/2} \xi^{2k} C_{2k,N}. \tag{22}$$

At this point we choose to model the ERBL region with these natural features in mind. We demand that the resultant GPDs reproduce the first moment $M_1 \approx 3$ and the second moment $M_2 \approx 1$ [37] [with the D term set to zero to remove the quadratic piece in Eq. (24)] where

$$M_1 = \int_0^1 dv H^{q,NS}(v,\xi) = 3, \tag{23}$$

$$M_2 = \int_0^1 dv v[H^{q,S}(v,\xi) + H^g(v,\xi)]$$

$$= 1 + C\xi^2 \tag{24}$$

and C in Eq. (24) was computed in the chiral-quark-soliton model [38]. This reasoning suggests the following simple analytical form for the ERBL region ($X < \zeta$):

$$\mathcal{F}^{g,NS}(X,\zeta) = \mathcal{F}^{g,NS}(\zeta)[1 + A^{g,NS}(\zeta) C^{g,NS}(X,\zeta)],$$

$$\mathcal{F}^{S}(X,\zeta) = \mathcal{F}^{S}(\zeta)\left(\frac{X-\zeta/2}{\zeta/2}\right)[1 + A^{S}(\zeta) C^{S}(X,\zeta)], \tag{25}$$

where the functions

$$C^{g,NS}(X,\zeta) = \frac{3}{2}\frac{2-\zeta}{\zeta}\left[1 - \left(\frac{X-\zeta/2}{\zeta/2}\right)^2\right],$$

$$C^{S}(X,\zeta) = \frac{15}{2}\left(\frac{2-\zeta}{\zeta}\right)^2\left[1 - \left(\frac{X-\zeta/2}{\zeta/2}\right)^2\right] \tag{26}$$

vanish at $X = \zeta$ to guarantee continuity of the GPDs. The $A^i(\zeta)$ are then calculated for each ζ by demanding that the first two moments of the GPDs are explicitly satisfied [remembering to include the D term in the ERBL region which only provides the quadratic term in ξ in Eq. (23)]. For the second moment what we do in practice is to set the D term to zero and demand that for each flavor the whole integral over the GPD is equal to the whole integral over the forward PDF for the input distribution concerned (due to the inherent small errors on the PDFs, the sum of such integrals will be close to, but not precisely equal to, unity). Note that the modeling of the ERBL region is unimportant at small ζ since the unknown subtraction constant in the dispersion relation, between the real part of the amplitude which formally depends on both the ERBL and the DGLAP region, and the imaginary part which formally depends only on the DGLAP region, is proportional to ζ and therefore inconsequential at small ζ.

It would be straightforward to extend this algorithm to satisfy polynomiality to arbitrary accuracy by writing the $A^i(\zeta)$ explicitly as a polynomial in ζ where the first few coefficients are set by the first two moments and the other coefficients are then randomly chosen since nothing is known about them. The above algorithm is extremely flexible in both its implementation and adaption to either other forward PDFs or other functional forms in the ERBL region. Therefore it can be easily incorporated into a fitting procedure.

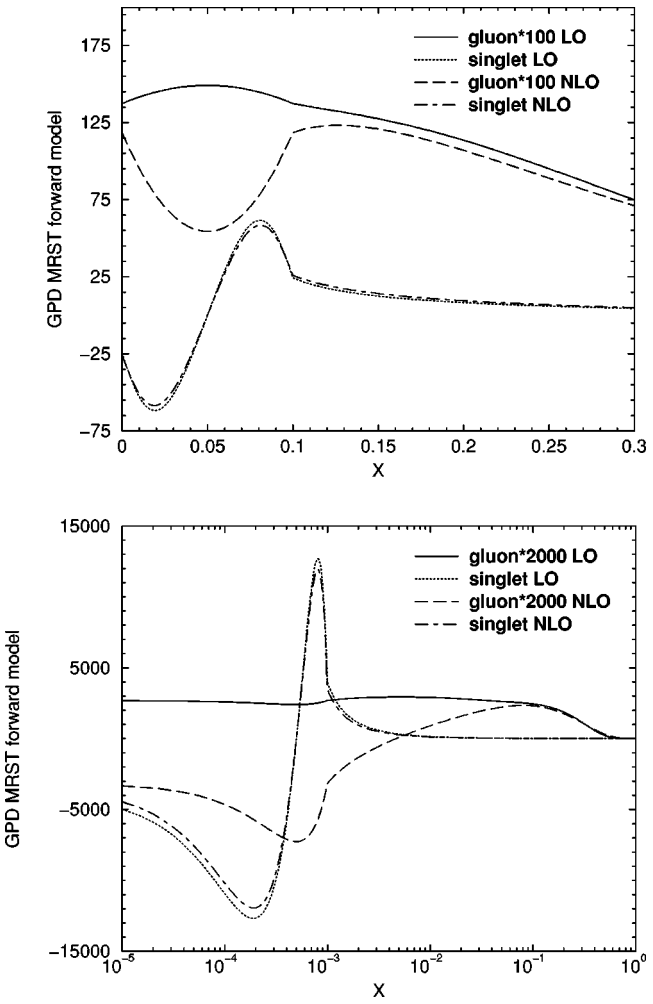

FIG. 8. The quark singlet and gluon GPDs in LO and NLO, using MRST01 input PDFs, at the input scale $Q_0 = 1$ GeV for $\zeta = 0.1$ (upper plot) and $\zeta = 0.001$ (lower plot), values typical of HERA and HERMES kinematics, respectively.

In Fig. 8 we show the shape of the resulting input GPDs for two characteristic values of $\zeta = 0.001, 0.1$. The upper plot in this figure explicitly shows the antisymmetry of the singlet GPD and the symmetry of the gluon GPD about the point $X = \zeta/2$.

The photon level cross section results from this model, using MRST01 [36] and CTEQ6 [39] input distributions at LO and NLO, are compared in Figs. 9 and 10 to the H1 [18] and ZEUS [35] data at their average kinematic points, respectively. In these curves we chose to use an x and Q^2-independent slope parameter of $B = 6.5\ \mathrm{GeV}^{-2}$, but realistically there is a 30–40 % uncertainty associated with the value of this unknown parameter. The figures illustrate that within the framework of the forward input model for GPDs the DVCS cross section remains rather sensitive to the choice of input PDF and to the accuracy with which the calculation is performed (i.e., LO or NLO). It should be

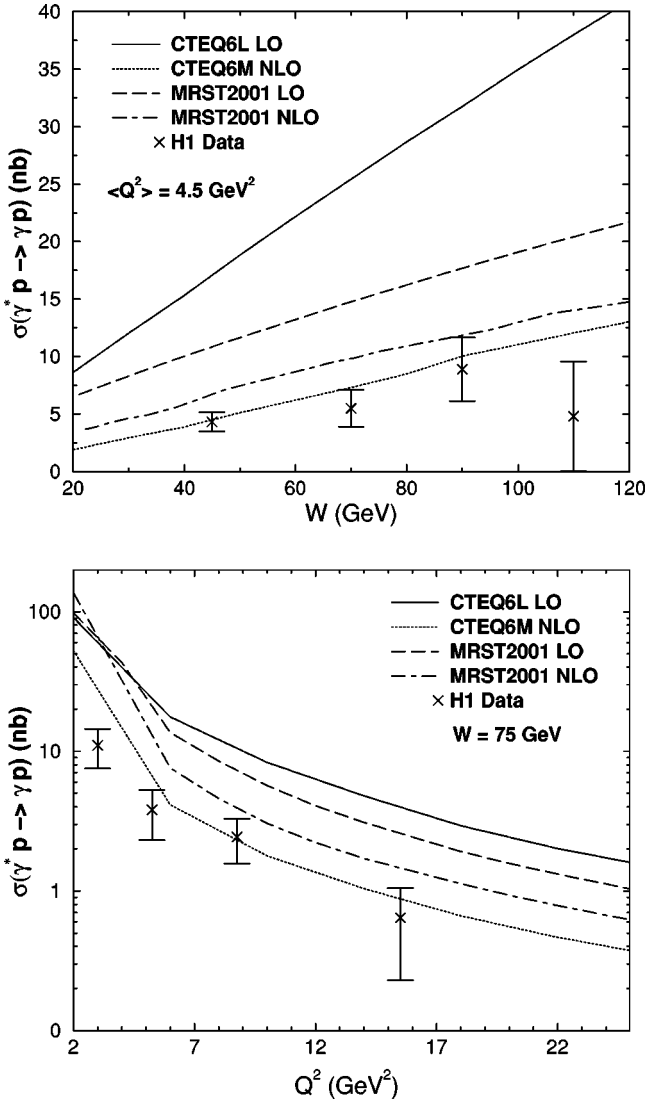

FIG. 9. The photon level cross section, $\sigma(\gamma^* p \to \gamma p)$, calculated using the forward model ansatz for input GPDs, in the average kinematics of the H1 data: as a function of W at fixed $Q^2 = 4.5$ GeV^2 (upper plot), and as a function of Q^2 at fixed $W = 75$ GeV (lower plot). A constant slope parameter of $B = 6.5$ GeV^{-2} was used.

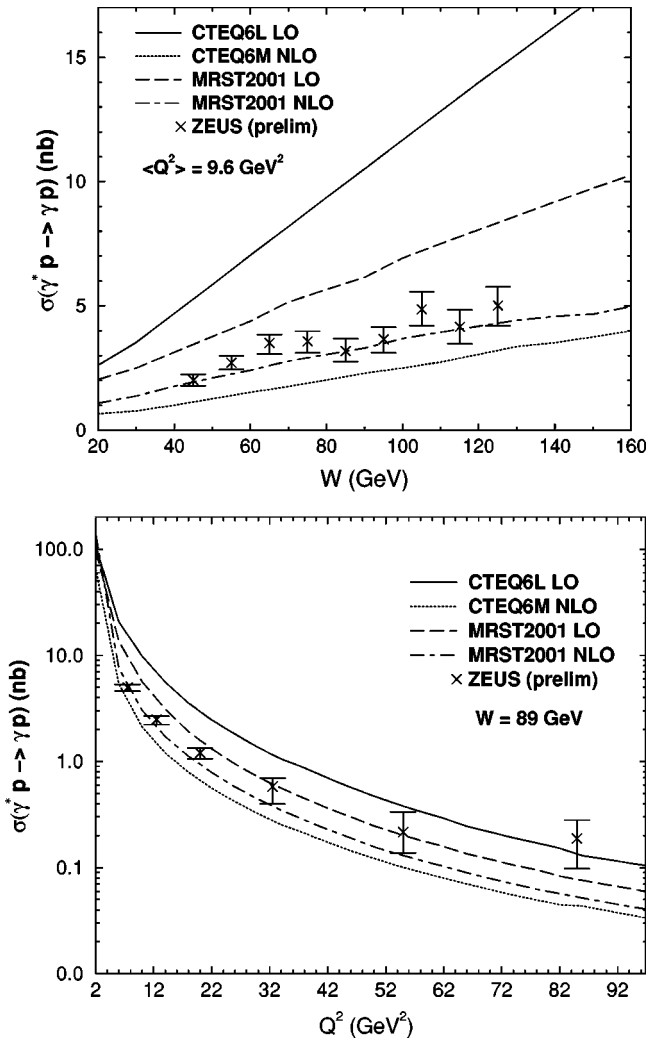

FIG. 10. The photon level cross section, $\sigma(\gamma^* p \to \gamma p)$, calculated using the forward model ansatz for input GPDs, in the average kinematics of the preliminary ZEUS data: as a function of W at fixed $Q^2 = 9.6$ GeV^2 (upper plot), and as a function of Q^2 at fixed $W = 89$ GeV (lower plot). A constant slope parameter of $B = 6.5$ GeV^{-2} was used.

noted that the description at the lowest H1 value of Q^2 is bad. However, the enhancement we chose using Eq. (21) at $Q_0^2 = 1$–1.69 GeV^2 corresponds more to the AJM at $Q^2 = 3$ GeV^2 (compare Figs. 6 and 7). Hence it is not surprising that the description at low Q^2 is not good, suggesting that the shift in X in Eq. (21) should be less at lower values of Q_0. When we increase the input scale of CTEQ6M, as done below, we find an appropriate reduction in the cross section at low Q^2 much more in line with the low Q^2 data and the AJM value.

It is important to note that the preliminary ZEUS data lie systematically above the H1 data (see Fig. 11 of [35]). Overall NLO seems to be doing better than LO, particularly on the slope of the energy dependence. It is fair to say that all of the theory curves appear to have a Q^2 dependence that is too steep to describe all of the data. We will return to this point in the next section.

The difference between the MRST and CTEQ curves at LO and NLO reflects the relative size of the quark singlet and gluon distributions for each set. It is possible that more precise data on DVCS may eventually allow a discrimination between various input scenarios using NLO QCD. For this to be realistic one would first need to pin down the uncertainty associated with the slope by explicitly measuring the t dependence.

We also investigated the effect on the cross section of increasing the input scale for skewed evolution using CTEQ input distributions, from the starting scale $Q_0 = 1.3$ GeV to $Q_0 = 2.0$ GeV. We then use the forward PDFs at the new scale in our model for the GPDs. Figure 11 shows that the reduced lever arm for skewed evolution starting at the higher scale leads to a smaller cross section at LO and NLO, as expected, and that, in LO at least, the effect of this change is

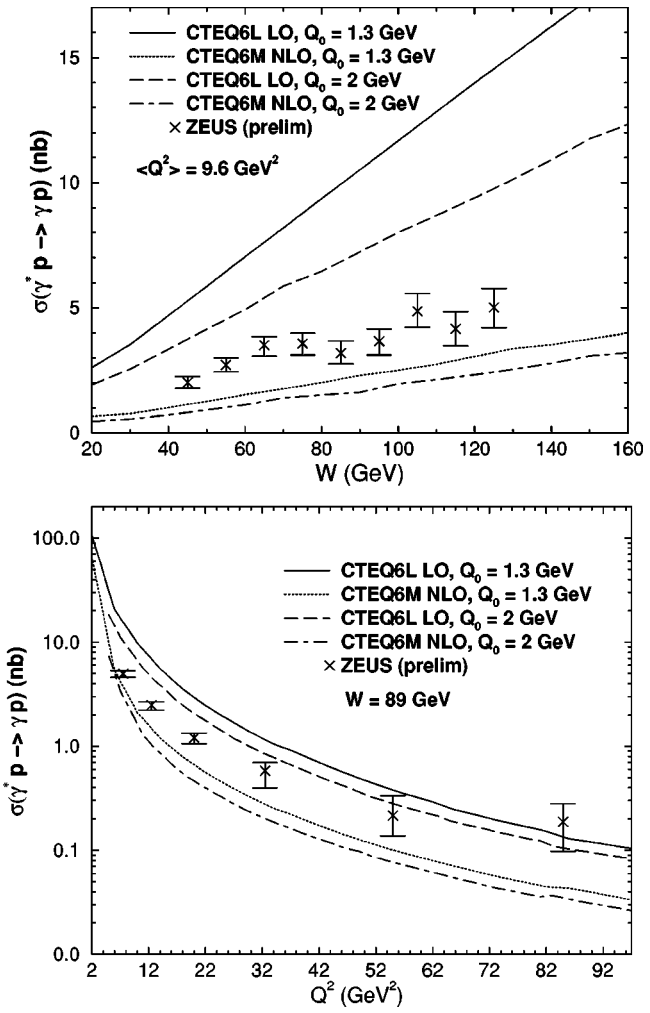

FIG. 11. The effect of changing the starting scale, Q_0, on photon level cross section $\sigma(\gamma^* p \to \gamma p)$, calculated using the forward model ansatz and CTEQ input PDFs, in the average kinematics of the preliminary ZEUS data: as a function of W at fixed $Q^2 = 9.6\ \mathrm{GeV}^2$ (upper plot), and as a function of Q^2 at fixed $W = 89\ \mathrm{GeV}$ (lower plot). A constant slope parameter of $B = 6.5\ \mathrm{GeV}^{-2}$ was used.

rather large. In fact the CTEQ and MRST Collaborations only advocate the use of their forward PDFs above $Q^2 \approx 3-4\ \mathrm{GeV}^2$ (they start evolution at a lower scale $Q^2 \approx 1-2\ \mathrm{GeV}^2$ due to technicalities associated with a consistent implementation of charm). Hence, it is not completely clear where one should start skewed evolution, and this constitutes an additional uncertainty in the theoretical predictions.

Having compared to small x_{bj} data we will now test the AJM ansatz for large x_{bj} by comparing to data on the single-spin asymmetry (SSA) (HERMES and CLAS [19]) and the charge asymmetry (CA) (HERMES only), defined by

$$\mathrm{SSA} = \frac{2\int_0^{2\pi} d\phi \sin(\phi)(d\sigma^{\uparrow} - d\sigma^{\downarrow})}{\int_0^{2\pi} d\phi (d\sigma^{\uparrow} + d\sigma^{\downarrow})},$$

$$\mathrm{CA} = \frac{2\int_0^{2\pi} d\phi \cos(\phi)(d\sigma^{+} - d\sigma^{-})}{\int_0^{2\pi} d\phi (d\sigma^{+} + d\sigma^{-})}. \tag{27}$$

Here $d\sigma^{\uparrow}, d\sigma^{\downarrow}$ refer to the differential cross sections with the lepton polarized along or against its direction of motion, respectively; $d\sigma^{+}, d\sigma^{-}$ are the unpolarized differential cross sections for positrons and electrons, respectively.

Such a comparison of QCD models with the available high x_{bj} data may be viewed with some skepticism, especially in the case of the CLAS data which have such a low $Q^2 \sim 1-2\ \mathrm{GeV}^2$ (HERMES data are only slightly better with a typical Q^2 of $\sim 2-4\ \mathrm{GeV}^2$). First, it is *a priori* not clear that perturbation theory is applicable at such low Q^2 values (in particular, higher twist corrections may be expected to become important in this region and our approximations correspond to the DVCS cross section being divergent as $Q^2 \to 0$). Secondly, the previously neglected GPDs $\tilde{H}$, E and $\tilde{E}$ become increasingly important as x increases [21,40]. In the following we will include the dominant twist-3 contributions [41], which are entirely kinematic in origin, in our calculation of the differential cross section, neglecting the subdominant twist-3 effects. We use the same input models for $\tilde{H}$, E and $\tilde{E}$ as well as t dependence for the various amplitudes i.e. various dipole form factors which are about equivalent with an exponential at small t with a slope B between 5 and 8, as in [21]. For HERMES we perform a full LO and NLO QCD analysis, whereas for CLAS we are restricting ourselves to LO, i.e., we are testing handbag dominance with no or little evolution. Furthermore, we shall restrict ourselves to MRST01 input PDF for simplicity.

It transpires that the average kinematics of HERMES is such that H is still the leading GPD and within our model assumptions $\tilde{H}$, E and $\tilde{E}$ could be set to zero for those values, with negligible difference to the final answer [43]. Within the above caveats, we find for average HERMES kinematics ($\langle x \rangle = 0.11, \langle Q^2 \rangle = 2.56\ \mathrm{GeV}^2, \langle t \rangle = -0.265\ \mathrm{GeV}^2$)

$$\mathrm{SSA} = -0.28\ \ (\mathrm{LO}), \quad -0.23\ \ (\mathrm{NLO}),$$

$$\mathrm{CA} = 0.12\ \ (\mathrm{LO}), \quad 0.09\ \ (\mathrm{NLO}), \tag{28}$$

compared to the quoted experimental results [44]

$$\mathrm{SSA} = -0.21 \pm 0.08,$$

$$\mathrm{CA} = 0.11 \pm 0.07. \tag{29}$$

For the average CLAS kinematics ($\langle x \rangle = 0.19, \langle Q^2 \rangle = 1.31\ \mathrm{GeV}^2, \langle t \rangle = -0.19\ \mathrm{GeV}^2$) we find

$$\mathrm{SSA} = 0.2\ \ (\mathrm{LO}) \tag{30}$$

compared to the experimental value (second reference of [19])

$$\mathrm{SSA} = 0.202 \pm 0.041. \tag{31}$$

This demonstrates that the AJM ansatz works surprisingly well even at large x_{bj} giving us confidence in the AJM-based model and suggesting that a fit to the available data should be possible without tuning too many input parameters.

IV. A SIMPLE MODEL FOR THE SLOPE PARAMETER

It was pointed out in [9] that the t slope of the DVCS cross section at small x should depend strongly on Q^2 in the transitional region from Q^2 of a few GeV^2 to large Q^2. At $Q^2 \sim 2\ \mathrm{GeV}^2$ it is natural to expect that the slope will be pretty close to that for exclusive ρ-meson production: $B \sim 8\ \mathrm{GeV}^{-2}$ [45]. For large Q^2 the dominant contribution is governed by evolution trajectories which, at the resolution $Q_0^2 \sim 2\ \mathrm{GeV}^2$, originate from the gluon field. Hence we expect that in this case the slope will be given by the square of the two-gluon form factor of the nucleon at $X, X-\zeta \gg x_{bj}$. Recently [46] it was demonstrated that for $x_{bj} \geqslant 0.05$ this t dependence can be approximated in a wide range of t as $1/(1-t/m_{2g}^2)^4$ with $m_{2g}^2 \sim 1.1\ \mathrm{GeV}^2$. This corresponds to a t slope of $B \sim 3\ \mathrm{GeV}^{-2}$ for exponential fits [47]. At smaller x an increase of the slope is expected which could originate from several effects, including Gribov diffusion. Hence for the highest Q^2 point of ZEUS of about 90 GeV^2 we expect $B = 3.5 \pm 0.5\ \mathrm{GeV}^{-2}$. The recent H1 and ZEUS ρ-meson production data, for a W range similar to the DVCS experiments, indicate that the slope of ρ production for both σ_L and σ_T drops rather rapidly with increasing Q^2 reaching $B \sim 5$ at $Q^2 \approx 10\ \mathrm{GeV}^2$ [48].

A simple parametrization which reflects the discussed constraints for the range of $2 \leqslant Q^2 \leqslant 100\ \mathrm{GeV}^2$ is

$$B(Q^2) = B_0 \left[1 - C \ln\left(\frac{Q^2}{Q_0^2} \right) \right] \tag{32}$$

with $B_0 = 8\ \mathrm{GeV}^{-2}$, $Q_0 = 2\ \mathrm{GeV}^2$, $C = 0.15$ being reasonable values for the various parameters. This gives $B(Q^2 = 9.6) = 6.1\ \mathrm{GeV}^{-2}$ and $B(Q^2 = 4.5) = 7.0\ \mathrm{GeV}^{-2}$ at the average Q^2 values of the ZEUS and H1 data, respectively (in broad agreement with our chosen constant value of $B = 6.5\ \mathrm{GeV}^{-2}$). Figure 12 illustrates the effect of introducing this simple model on the description of the Q^2 dependence of the ZEUS data.

This modification of the B slope gives a great improvement in comparison with the data and shows how important an experimental determination of the B slope is, since it constitutes a large theoretical uncertainty at this point.

V. CONCLUSIONS

Using sound phenomenological guidelines such as the aligned jet model, we have constructed a model for generalized parton distributions at the input scale. Within certain theoretical uncertainties (such as the exact shape, the input scale and the functional form of B in W and Q^2) this model can be used in a NLO QCD analysis to describe the recent DVCS data from the H1, ZEUS, HERMES, and CLAS experiments within their experimental errors. In constructing this model we have given a simple and flexible algorithm which can be easily incorporated into a fitting procedure.

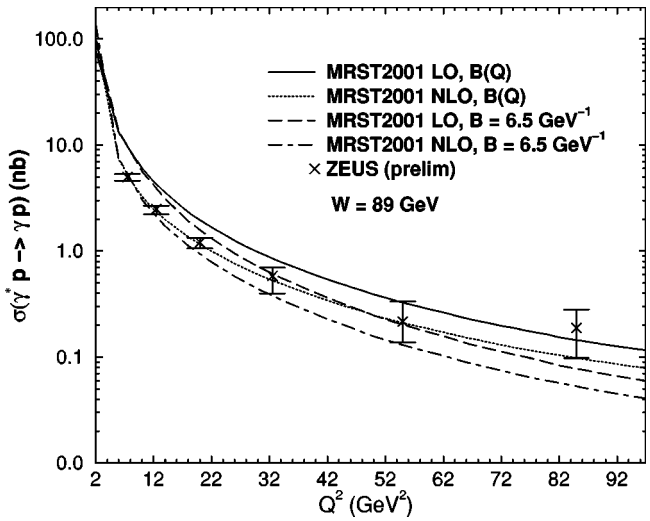

FIG. 12. The effect on the DVCS cross section, in the average kinematics of the ZEUS data, of introducing our simple Q^2-dependent model of Eq. (32) for B, the slope of the t dependence.

We have also demonstrated and explained the failure of the most widely used model for generalized parton distributions, the factorized double distribution based model, to describe the available DVCS data, when rigorously applied in a LO or NLO QCD analysis in its current form.

The modeling of the input GPDs is now sufficiently advanced to justify attempting to fit some of the input parameters directly to the available data. A basic analysis of the data would seem to favor a t dependence with a slope parameter, B, that depends on Q^2. Hence, an accurate measurement of this slope is of crucial importance for further progress of the comparison of theory and experiment.

ACKNOWLEDGMENTS

We would like to thank H. Abramowicz, C. Weiss, M. Diehl, L. Frankfurt, K. Golec-Biernat, D. Müller, and A. Schäfer for helpful discussions. A.F. was supported by the DFG Emmi-Noether Program, M.M. by PPARC, and M.S. by the DOE.

[1] D. Müller *et al.*, Fortschr. Phys. **42**, 101 (1994).
[2] X. Ji, Phys. Rev. D **55**, 7114 (1997); J. Phys. G **24**, 1181 (1998).
[3] A.V. Radyushkin, Phys. Rev. D **56**, 5524 (1997).
[4] M. Diehl *et al.*, Phys. Lett. B **411**, 193 (1997).
[5] Müller [1].
[6] M. Vanderhaeghen, P.A.M. Guichon, and M. Guidal, Phys. Rev. D **60**, 094017 (1999).

[7] J.C. Collins and A. Freund, Phys. Rev. D **59**, 074009 (1999).
[8] L. Frankfurt *et al.*, Phys. Lett. B **418**, 345 (1998); **429**, 414(E) (1998); A. Freund and V. Guzey, *ibid.* **462**, 178 (1999).
[9] L. Frankfurt, A. Freund, and M. Strikman, Phys. Rev. D **58**, 114001 (1998); **59**, 119901(E) (1999); Phys. Lett. B **460**, 417 (1999); A. Freund and M. Strikman, Phys. Rev. D **60**, 071501 (1999).
[10] K.J. Golec-Biernat and A.D. Martin, Phys. Rev. D **59**, 014029 (1999).
[11] A.G. Shuvaev *et al.*, Phys. Rev. D **60**, 014015 (1999); K.J. Golec-Biernat, A.D. Martin, and M.G. Ryskin, Phys. Lett. B **456**, 232 (1999).
[12] A.V. Belitsky, and D. Müller, Phys. Lett. B **417**, 129 (1998); Nucl. Phys. **B537**, 397 (1999); Phys. Lett. B **464**, 249 (1999); Nucl. Phys. **B589**, 611 (2000); Phys. Lett. B **486**, 369 (2000); A.V. Belitsky, A. Freund, and D. Müller, *ibid.* **461**, 270 (1999); Nucl. Phys. **B574**, 347 (2000); Phys. Lett. B **493**, 341 (2000).
[13] Regular parton distributions are merely particle distributions not particle correlation functions.
[14] M.V. Polyakov and C. Weiss, Phys. Rev. D **60**, 114017 (1999).
[15] Factorized refers here to writing the DD, a three-variable function, in terms of the product of a two-variable with two one-variable functions as explicitly shown in Sec. II.
[16] A.V. Radyushkin, Phys. Rev. D **59**, 014030 (1999).
[17] A.V. Radyushkin, Phys. Lett. B **449**, 81 (1999).
[18] H1 Collaboration, C. Adloff *et al.*, Phys. Lett. B **517**, 47 (2001).
[19] HERMES Collaboration, A. Airapetian *et al.*, Phys. Rev. Lett. **87**, 182001 (2001); CLAS Collaboration, S. Stepanyan *et al.*, *ibid.* **87**, 182002 (2001).
[20] A. Freund and M. McDermott, Phys. Rev. D **65**, 091901(R) (2002).
[21] A. Freund and M. McDermott, Eur. Phys. J. C **23**, 651 (2002).
[22] A.V. Belitsky *et al.*, Nucl. Phys. **B629**, 323 (2002).
[23] J.D. Bjorken *et al.*, Phys. Rev. D **8**, 1341 (1973).
[24] L.L. Frankfurt and M.I. Strikman, Phys. Rep. **160**, 235 (1988); Nucl. Phys. **B316**, 340 (1989).
[25] A. Freund and M. McDermott, Phys. Rev. D **65**, 074008 (2002).
[26] A.V. Belitsky, D. Müller, L. Niedermeier, and A. Schäfer, Nucl. Phys. **B546**, 279 (1999); Phys. Lett. B **437**, 160 (1998); A.V. Belitsky, B. Geyer, D. Müller, and A. Schäfer, *ibid.* **421**, 312 (1998).
[27] I.V. Musatov and A.V. Radyushkin, Phys. Rev. D **61**, 074027 (2000).
[28] The fact that $\pi(x,y)=\pi(x,-y)$ guarantees that odd powers of ξ are missing from the moments of $H(v,\xi)$. This is required by Hermiticity and time reversal of the corresponding hadronic matrix elements.
[29] Comparison of any of the above models with data from the HERMES and CLAS experiments shows that the same problem persists also for large x_{bj}, as already pointed out in [20].
[30] A.V. Belitsky *et al.*, Phys. Lett. B **510**, 117 (2001).
[31] A. Freund and M. McDermott, Phys. Rev. D **65**, 056012 (2002).
[32] A.V. Belitsky, D. Müller, L. Niedermeier, and A. Schäfer, Phys. Lett. B **474**, 163 (2000).
[33] M. Glück, E. Reya, and A. Vogt, Eur. Phys. J. C **5**, 461 (1998).
[34] ZEUS Collaboration, P.R. Saull, ''Prompt Photon Production and Observation of Deeply Virtual Compton Scattering,'' Proceedings of ICHEP1999, Tampere, Finland, 1999, hep-ex/0003030.
[35] ZEUS Collaboration, ''Measurement of the Deeply Virtual Compton Scattering Cross Section at HERA,'' contributed paper, abstract 825, to ICHEP2002, Amsterdam, 2002.
[36] A.D. Martin *et al.*, Eur. Phys. J. C **23**, 73 (2002).
[37] The first moment counts the number of quarks in the proton and the second moment is a generalization of the momentum sum rule where the D term generates all the deviation from unity as ξ varies.
[38] N. Kivel, M.V. Polyakov, and M. Vanderhaeghen, Phys. Rev. D **63**, 114014 (2001).
[39] CTEQ Collaboration, J. Pumplin *et al.*, J. High Energy Phys. **07**, 012 (2002).
[40] A.V. Belitsky *et al.*, Nucl. Phys. **BB593**, 289 (2001).
[41] A.V. Belitsky, D. Müller, and A. Kirchner, Nucl. Phys. **B629**, 323 (2002).
[42] H1 Collaboration, Eur. Phys. J. C **21**, 33 (2001).
[43] At very small t, $\widetilde{\mathrm{E}}$ becomes large due to the pion pole it contains. However, due to other kinematical factors in front of it, the contribution from the term involving $\widetilde{\mathrm{E}}$ only becomes important close to t_{min}, which is never reached at either the HERMES or CLAS experiment.
[44] HERMES Collaboration, F. Ellinghaus *et al.*, Nucl. Phys. **A711**, 171 (2002).
[45] ZEUS Collaboration, ''Exclusive and Proton-Dissociative Electroproduction of ρ^0 Mesons at HERA,'' contributed paper, abstract 818, to ICHEP2002, Amsterdam, 2002.
[46] L. Frankfurt and M. Strikman, Phys. Rev. D **66**, 031502(R) (2002).
[47] One needs to investigate how a change of the t-slope parametrization in the Monte Carlo simulation used to analyze the ZEUS and H1 data would modify the extracted cross section.
[48] H1 Collaboration, ''Elastic Electroproduction of ρ Mesons at High Q^2 at HERA,'' contributed paper, abstract 989, to ICHEP2002, Amsterdam, 2002.